Supporting Information

Resonance Raman Analysis of the Tryptophan Cation Radical

Hannah S. Shafaat[‡] *and Judy E. Kim**

[‡]Currently at The Ohio State University

Department of Chemistry and Biochemistry, University of California at San Diego

judyk@ucsd.edu

Table of Contents

Rapid mixing device

The rapid mixing device was assembled from commercial components (Figure S1). A Y-union connector (PN P-512, Upchurch Scientific) was bolted to an anodized aluminum base (Thorlabs BA2) and connected via 250 μm i.d. PEEK tubing (Upchurch Scientific) to a 450 μm o.d., 320 μm i.d. quartz microcapillary. Solutions were pumped to the mixing device via a dual port syringe pump (KD Scientific); the time delay following mixing was controlled by the rate of dispensation from the syringe pump. It was found that a rate of 100 μL/min for each solution gave the highest signal, which corresponds to a linear flow rate of ~40 mm/s and a mixing time of ~1 s measured ~ 4 cm away from the mixing region. Spectra were collected with variable mixing times from ~100 ms to ~2 s in order to enhance S/N for a particular experiment (Figure S2). All signal disappeared if the solution was not flowing.

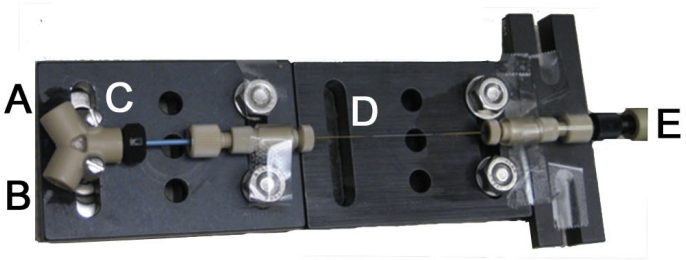

Figure S1. Mixing device used for resonance Raman experiments. Solutions were introduced into the device at ports A and B and mixed at point C. The laser beam probed the mixed samples at point D, and waste was collected at point E.

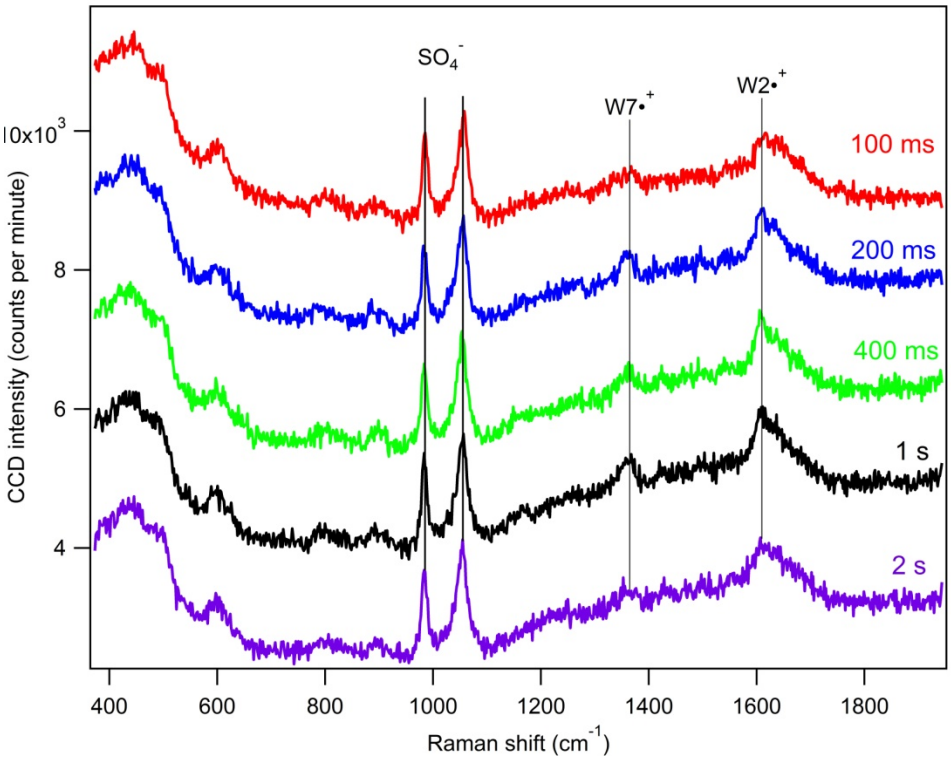

Figure S2. Single 1-minute spectra of 1 mM $Ce^{IV}(SO_4)_2$ + 1 mM L-Trp in 225 mM H_2SO_4 probed at varying delay times from 100 ms to 2 s (variable flow rates from 0.05 to 1 mL/min). Observed sulfate and $TrpH^{\bullet+}$ peaks are indicated.

Resonance Raman Spectroscopy

Resonance Raman spectroscopy was performed with a homebuilt Raman microscope system. A mixed-gas Kr-Ar laser (Coherent Innova 70C) provided excitation at 458.0 nm, 488.0 nm, 514.5 nm, and 568.2 nm. The 40-70 mW beam was sent through an interference filter (Semrock) for the appropriate wavelength and directed into a modified fluorescence alignment port of a Zeiss Axio Imager A1m upright microscope. A broadband beamsplitter (Edmund Optics) directed a small portion (~10%) of the beam downward to the entrance aperture of a 10x objective. The power at the sample was ~2.5-3.5 mW. Back-scattered light was collected and collimated with the same objective and passed through the beamsplitter to the microscope sideport. The light was focused onto a 100 μm entrance slit and Rayleigh light was rejected using the appropriate long-pass edge filter (Semrock RazorEdge). Raman scattered light was dispersed in an f/5 0.32 m spectrograph (Horiba Jobin Yvon iHR-320) equipped with a 1200 grooves/mm grating blazed at 500 nm (default) or 2400 grooves/mm grating blazed at 400 nm (high resolution, indicated when utilized) and imaged onto a Peltier-cooled CCD (Horiba Jobin Yvon Synapse). The spectral bandpass was <10 cm^{-1} for the 1200 gr/mm grating and <5 cm^{-1} for the 2400 gr/mm grating. Wavelength calibration was performed using ethanol for the 1200 gr/mm grating, and a Ne lamp (Oriel Pen Lamp PN 6032) for the 2400 gr/mm grating. Spectral accuracy was ± 1 cm^{-1} and ± 0.5 cm^{-1} for the 1200 gr/mm and 2400 gr/mm grating, respectively. Spectra were not corrected for instrument response; however, because this spectral window is in the middle of the visible range, where the optical components and CCD are optimized, a qualitative analysis indicates that <10% change in resonance Raman intensities is anticipated across the entire spectral window.

Spectra of blank and sample solutions were obtained to isolate peaks from the tryptophan cation radical. Blank spectra were generated by mixing 225 mM sulfuric acid with either 1 mM tryptophan derivative in 225 mM sulfuric acidor cerium sulfate in 225 mM sulfuric acid. These mixtures gave similar results, and exhibit signal from solvent and other reagents, such as sulfate, but do not contain signal from tryptophan cation radical. The blank spectrum was then subtracted from the spectra of 1 mM tryptophan derivative in 225 mM sulfuric acid mixed with 1 mM cerium sulfate in 225 mM sulfuric acid. Spectra were collected for ~3 hrs for each sample and blank solution. The blank spectra were multiplied by a scalar such that the desired subtraction of (sample − blank) contained minimal contributions from the strong sulfate peaks at 980 cm^{-1} and 1055 cm^{-1}. Resonance Raman intensities were determined using the isolated 980 cm^{-1} sulfate peak as an internal standard. Data analysis was carried out using IGOR Pro v.6.23 (Wavemetrics, Lake Oswego, OR). High resolution spectra were smoothed with a 5 point Savitsky-Golay algorithm.

UV resonance Raman Spectroscopy

Instrumentation for ultraviolet resonance Raman spectroscopy has been described in detail elsewhere.[1] Briefly, a 1 kHz Ti:Sapphire laser (Photonics Industries) provided >1-Watt beam at 912 nm; the fundamental was directed through a lithium triborate (LBO) crystal, and the resulting 456 nm beam was then passed through a β-barium borate (BBO) crystal to produce > 6 mW of 228 nm UV excitation. The UV beam was focused with a pair of cylindrical lenses to a spot size of ~230 μm x ~75 μm at the sample. The power at the sample was ~3 mW. Scattered light was collected in a ~135° backscattering geometry and focused onto the entrance slit of a prism-based prefilter. Raman scattered light was dispersed in a 0.5 m spectrograph (JY Horiba,

Spex 500M equipped with a 3600 gr/mm holographic grating), and imaged onto a CCD detector (Princeton Instruments, Pixis 400B). The spectral response was determined by a deuterium lamp, and the bandpass (~10 cm^{-1}) and accuracy (~1 cm^{-1}) were determined from ethanol calibration spectra. Previous UVRR power dependence studies indicated that the current experiments were performed under conditions of linear response (data not shown).[2]

Samples were pumped through a vertically-oriented, 100 μm i.d. quartz microcapillary at a linear flow rate of 340 μm/ms to ensure fresh sample for each laser pulse, and discarded after a single-pass through the laser beam to eliminate artifacts from photolyzed sample. Fifteen-minute UVRR spectra were collected for ~50 μM tryptophan derivative samples under the following buffer conditions: 20 mM phosphate buffer H_2O at pH 7.2, 20 mM phosphate buffer (D_2O) at pD 7.6, 225 mM H_2SO_4 in H_2O and 225 mM D_2SO_4 in D_2O. Spectra of buffer-only solutions were also acquired and subtracted from corresponding sample spectra. All spectra were normalized to peak intensity and offset for presentation clarity in the main text figures.

Absorption spectroscopy

Absorption spectroscopy was carried out using a UV-Vis spectrophotometer (HP 8453). Absorption spectra of 1 mM NATA and 1 mM cerium sulfate in 225 mM H_2SO_4 following rapid mixing were obtained in a polycarbonate 1 cm pathlength cuvette equipped with ports for a flow system (Malvern Instruments DTS1061). Due to limitations of the connectors and the syringe pump, the maximum flow rate was 1 mL/min, which corresponds to a linear flow rate of 1 mm/s. We were unable to monitor the ground state absorption of NATA at ~280 nm region because the material was not transparent in the UV region.

Calculations

Calculations were performed using the Gaussian 09W quantum chemistry program operating on a Windows platform.[3] The geometry and harmonic vibrational frequencies of L-tryptophan and NATA were calculated using DFT with the hybrid B3LYP functional. Calculations for the L-tryptophan and NATA cation radicals were performed using spin-unrestricted DFT with the B3LYP functional. A 6-31+G basis set was selected for all calculations. Molecular orbitals were generated and viewed using GaussView.[3]

Mode assignments

Mode assignments for the observed peaks of the tryptophan cation radical were made by comparing results from calculations of closed-shell NATAH to the N-acetyltryptophanamide cation radical ($NATAH^{\bullet+}$) with the aid of software to visualize atomic displacements[4] as described in detail previously.[5] Vibrational modes were assigned based on visual match of the nuclear displacements of the indole ring as well as calculated mode similarities. Peaks were assigned on the basis of their predicted frequencies as well as the calculated and measured isotope shifts. Unless otherwise noted, nomenclature used here follows standard mode descriptions in the literature.[6]

Control measurements of absorption spectra

In order to confirm that any irreversible waste product following mixing of NATA with cerium sulfate was not responsible for the observed RR spectra, absorption spectra of the reagents and waste were obtained (Figure S6). Following reduction of Ce(IV) by NATA, the strong absorption of Ce(IV) in aqueous solution at 318 nm disappeared, indicating that the

Ce(III) species was formed irreversibly. The waste product showed a small new absorption at 452 nm, which may represent either the absorption of the Ce(III) product or possible irreversible degradation of NATAH•$^{+}$. Because all vibrational peaks attributed to NATAH•$^{+}$ disappeared over time if the reactants were not flowing through the mixer, the long-lived species with a weak absorption at 452 nm is not responsible for the transiently-observed bands. Only small decreases in the absorption features of closed-shell NATAH are seen after mixing with Ce(IV).

Effects of using larger molecule for normal mode calculations

Our approach is to use a more complicated molecule, NATA, rather than simply indole, 3-methylindole, or 3-ethylindole (3EI) to guide normal mode assignments.[7-10] The use of a larger structural model that includes the backbone in the normal mode calculations will likely have a significant effect on the tryptophan cation radical; in this species, the electronic transition involves changes in electronic density on atoms away from the indole ring.[11] Calculations also predict spin delocalization onto the backbone atoms for the tryptophan cation radical in a number of conformations, though this is not found for the tryptophan neutral radical.[12] This delocalization is in accordance with what has been observed for the EPR and FT-IR spectra of tyrosyl radicals in proteins and model compounds, where the spin delocalizes onto the backbone nitrogen, and isotopic substitution impacts vibrational band positions.[13, 14] Therefore, any normal modes with significant displacement of these atoms in response to the electronic transition will contribute to the resonance Raman spectrum. Graphical depictions of calculated NATA normal modes for the closed-shell and cation radical (NATAH•$^{+}$) species are shown in Figures S9 and S10; comparison between calculated and assigned frequencies for both NATA and NATAH•$^{+}$ are given in Table S1.

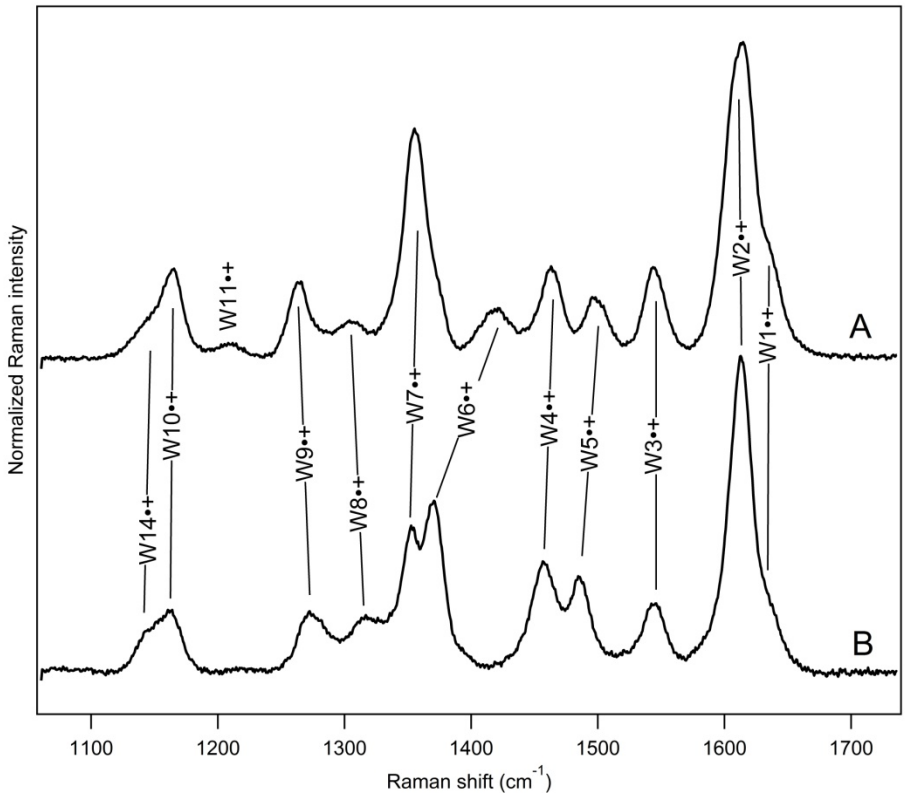

Figure S3. High resolution visible resonance Raman spectra (514.5 nm excitation, 2400 gr/mm grating) and normal mode assignments of (A) $NATAH^{\bullet+}$ in 225 mM H_2SO_4 in the presence of 500 μM $Ce^{IV}(SO_4)_2$ and (B) $NATAD^{\bullet+}$ in 225 mM D_2SO_4 in the presence of 500 μM $Ce^{IV}(SO_4)_2$.

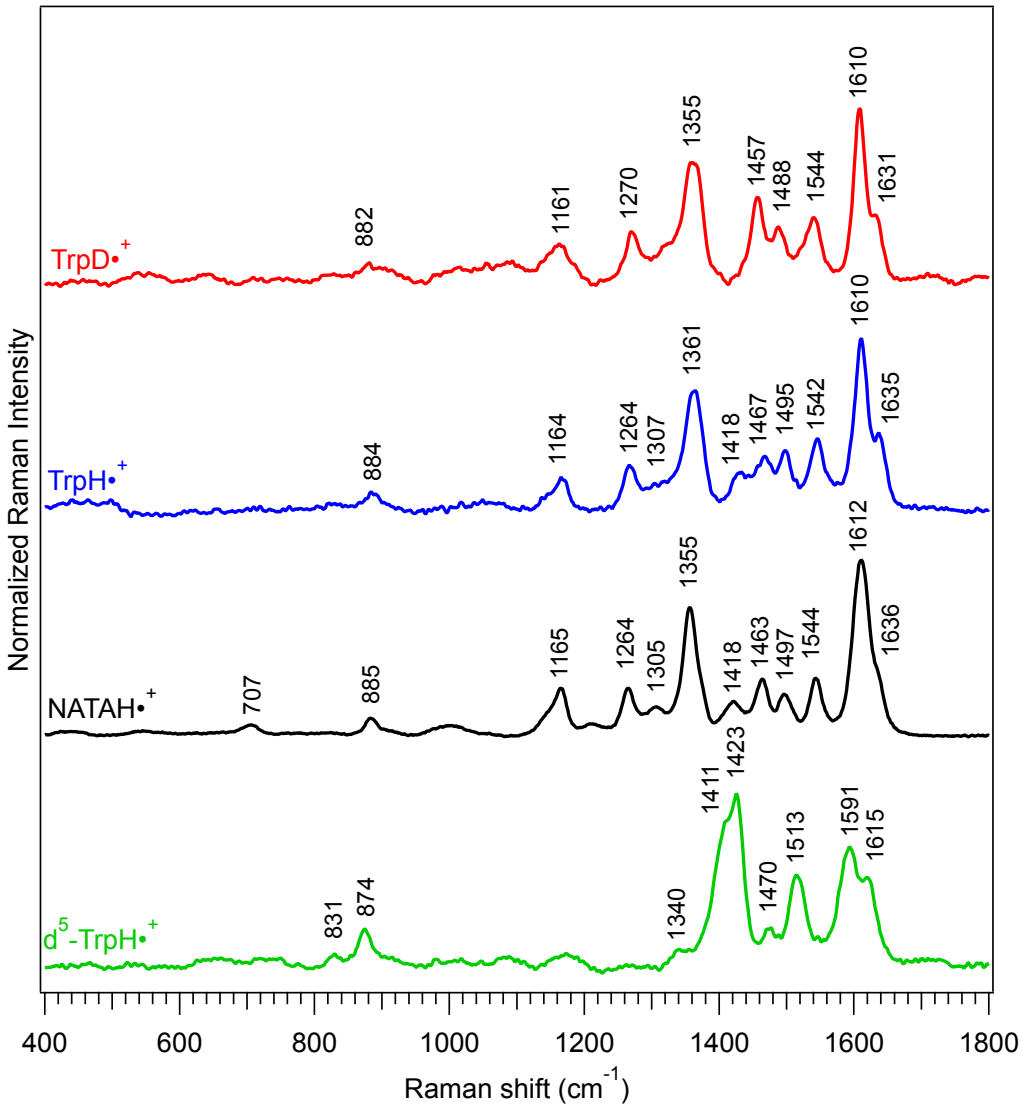

Figure S4. Visible resonance Raman spectra (514.5 nm excitation) of TrpD•$^{+}$, TrpH•$^{+}$, NATAH•$^{+}$, and d^{5}-TrpH•$^{+}$ in 225 mM sulfuric acid in the presence of 500 µM $Ce^{IV}(SO_4)_2$.

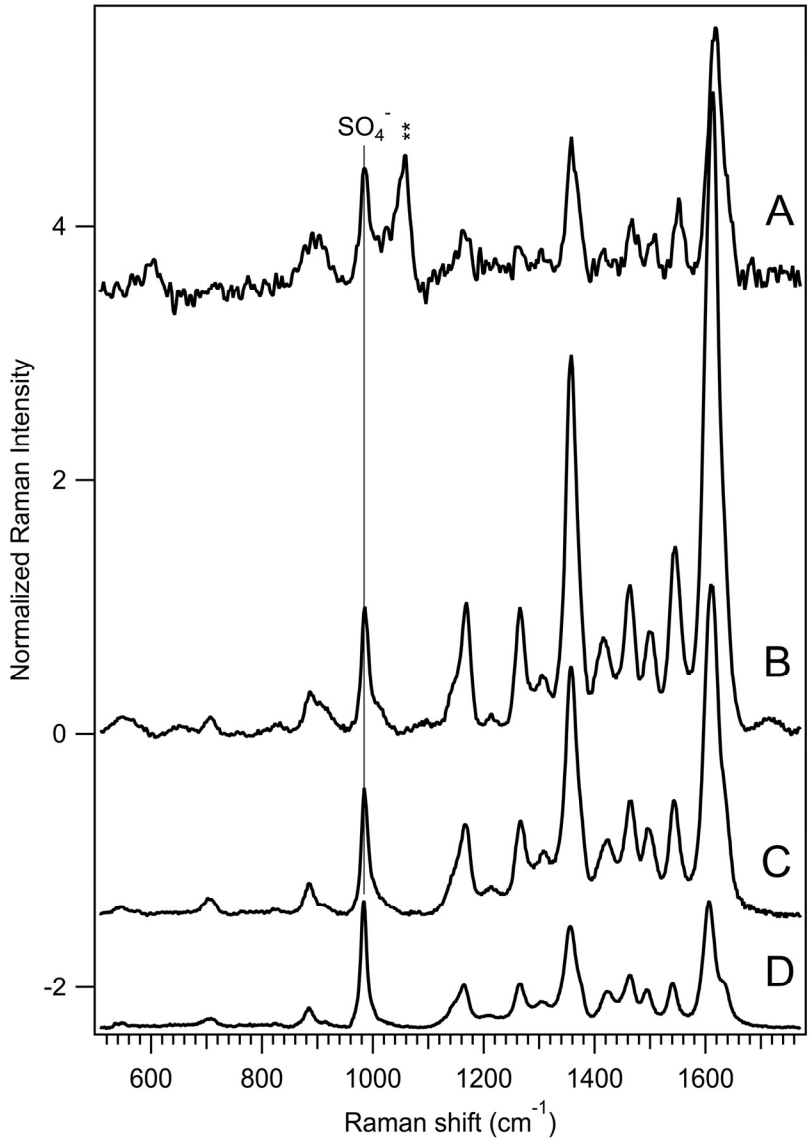

Figure S5. Resonance Raman spectra of NATAH•$^{+}$ in 225 mM sulfuric acid in the presence of 500 μM $Ce^{IV}(SO_4)_2$ with excitation wavelengths (A) 458.0 nm, (B) 488.0 nm, (C) 514.5 nm, and (D) 568.2 nm. Spectra are normalized to the 980 cm^{-1} band of sulfate (indicated). Spectrum A has been smoothed with a 5 point Savitzky-Golay algorithm. The 1055 cm^{-1} sulfate peak has been removed in spectra (B) thru (D) by isolating this region in the blank spectra, and subtracting this isolated sulfate peak from the sample spectra; this analysis was not performed for spectrum (A) because of low S/N, and the peak is indicated with (**).

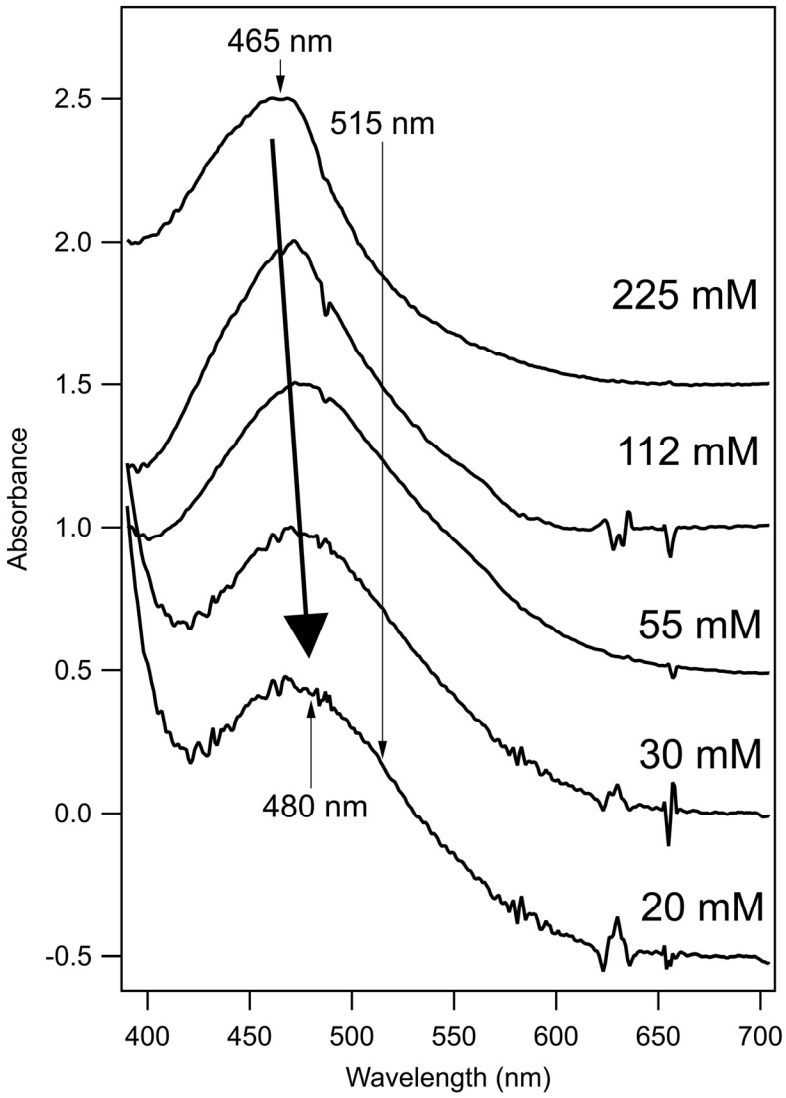

Figure S6. Absorption spectra of 1 mM NATAH + 1 mM $Ce^{IV}(SO_4)_2$ in varying sulfate concentrations of 20 to 225 mM. The flow rate of the solutions was 200 µL/min, which corresponds to a linear flow rate of ~0.2 mm/s and a probe time of 30 seconds after mixing. Probe times as low as 3 seconds were measured and found to give approximately the same results, but with greater noise. Evolutions of peak maxima and absorption shoulder are indicated on graph.

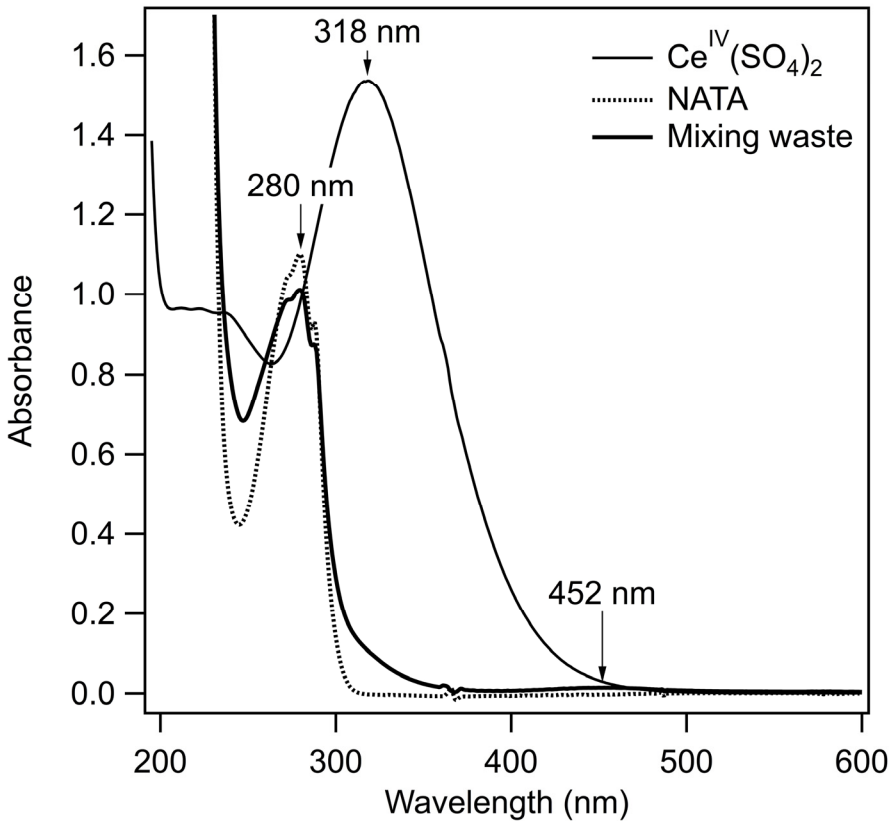

Figure S7. Absorption spectra of 500 μM NATAH in 225 mM H_2SO_4 (dotted), 330 μM $Ce^{IV}(SO_4)_2$ in 225 mM H_2SO_4 (thin solid), and the waste generated ~2 hrs after mixing of 1 mM NATA in 225 mM H_2SO_4 with 1 mM CeSO4 in 225 mM H_2SO_4 for resonance Raman experiment (thick solid). Spectra were measured in a 4 mm pathlength quartz cuvette.

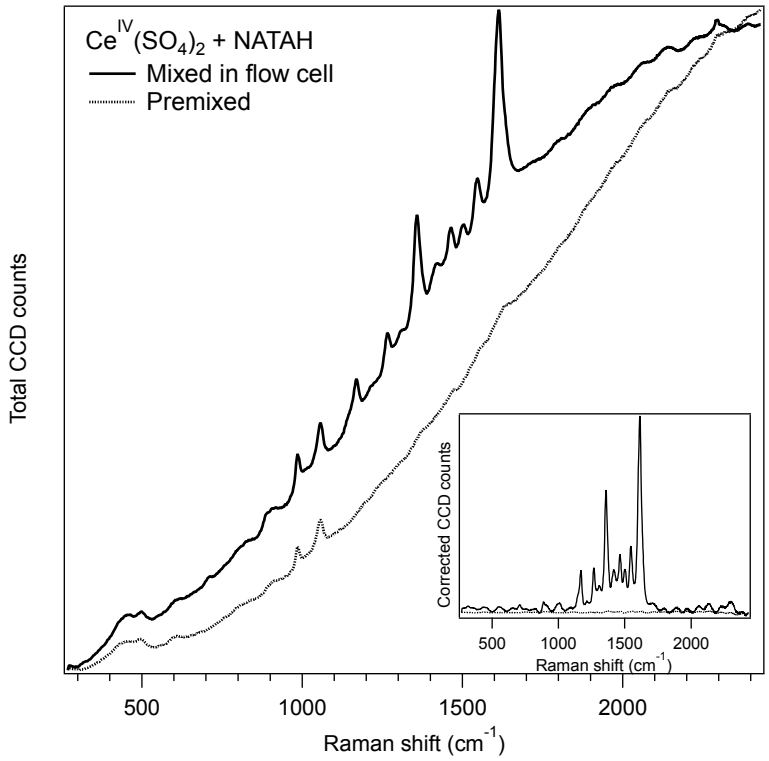

Figure S8. Uncorrected RR spectra (488.0 nm excitation) of a mixture of NATAH and Ce(IV) (1 mM NATA in 225 mM H_2SO_4 with 1 mM $Ce^{IV}(SO_4)_2$ in 225 mM H_2SO_4). Regents were mixed in the flow cell (solid), or pre-mixed for a period of one hour before flowing through the cell (dotted). (*Inset*) Resulting spectra after subtracting solvent peaks and broad background. Intense positive peaks reflect tryptophan cation radical that is only formed when NATAH and Ce(IV) are mixed in the cell.

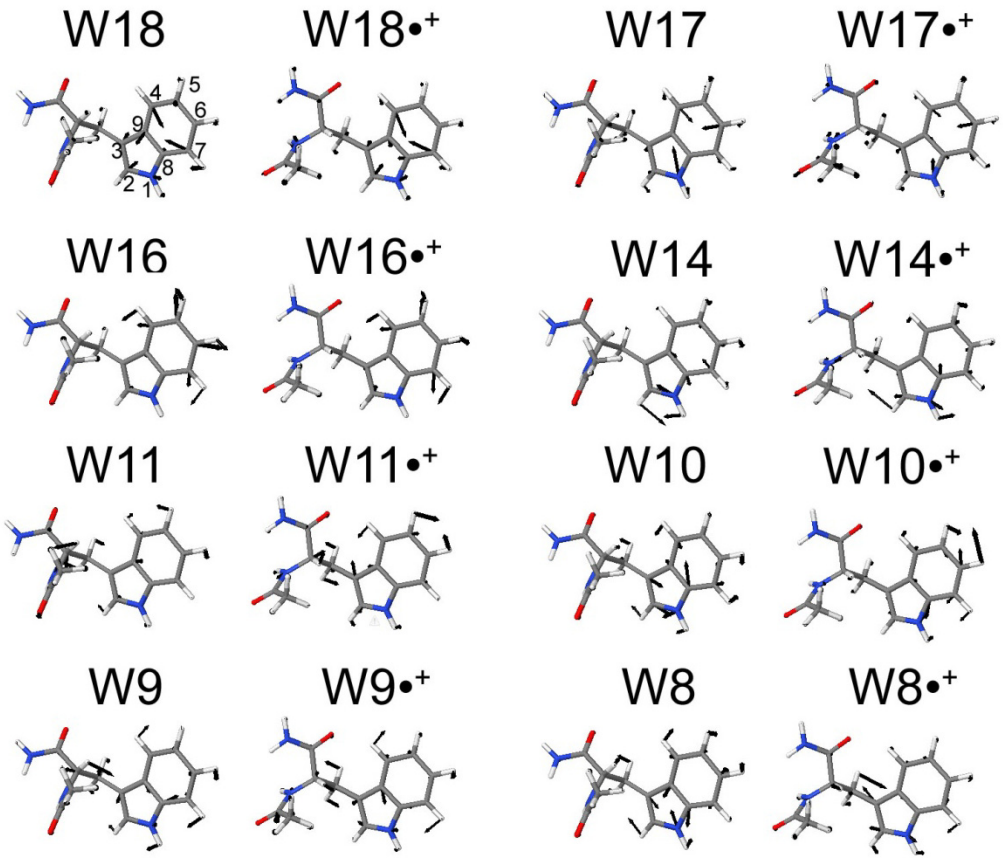

Figure S9. Calculated N-acetyltryptophanamide low-frequency normal modes for the closed shell (NATAH) and cation radical (NATAH•$^{+}$) species. Mode numbering is as described in the literature.[6] All displacements are in the plane of the indole ring. Atomic numbering scheme referred to in the text is shown on mode W18.

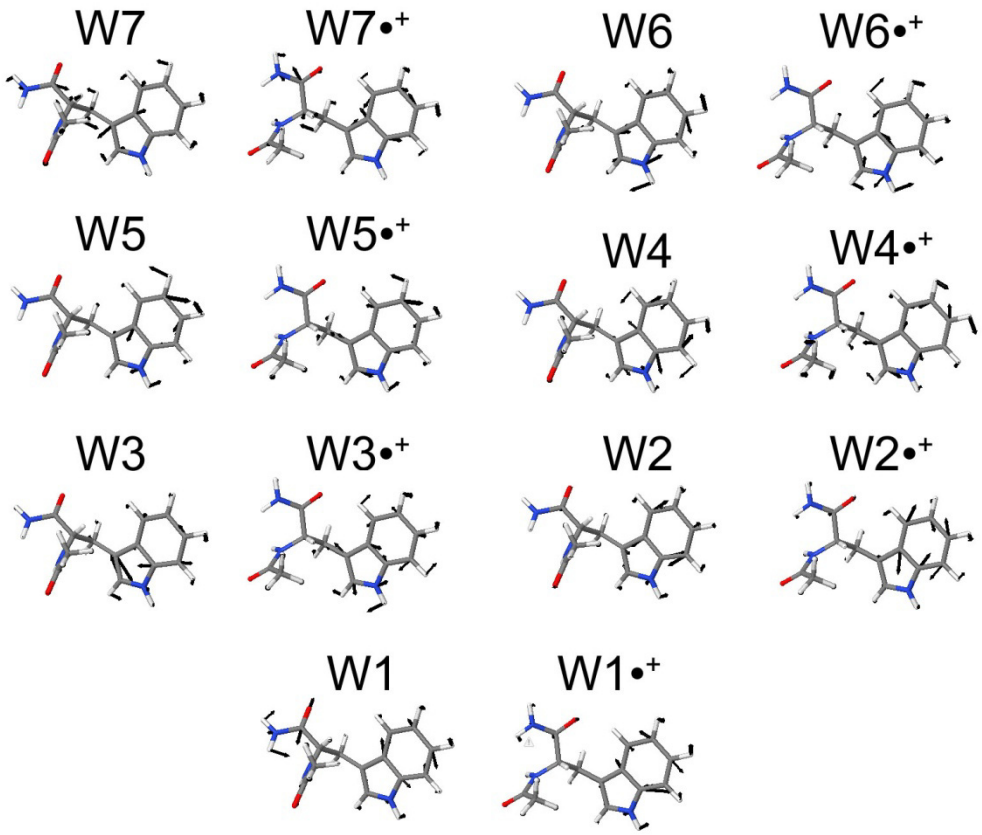

Figure S10. Calculated N-acetyltryptophanamide high-frequency normal modes for the closed shell (NATAH) and cation radical (NATAH•$^{+}$) species. Mode numbering is as described in the literature.[6] All displacements are in the plane of the indole ring.

Mode	NATAH mode#	ν_{NATAH} calc.	ν_{NATAH} obs.	% Error	NATAH•$^{+}$ mode#	$\nu_{NATAH•+}$ calc.	$\nu_{NATAH•+}$ obs.	% Error	Mode similarity
W18	40	777	761	-2.1%	40	773.4	707	-8.6%	46.2%
W17	45	903	883	-2.2%	43	881	885	0.5%	64.8%
W16	51	1044	1012	-3.0%	50	1039	NA		86.9%
W14	56	1126	1078	-4.2%	58	1178	1145	-2.8%	49.6%
W13	58	1169	1127	-3.6%	56	1113	NA		36.3%
W12	59	1210	1156	-4.5%	60	1222	NA		44.3%
W11	60	1236	1203	-2.7%	61	1246	1210	-2.9%	55.8%
W10	61	1265	1238	-2.1%	59	1216	1165	-4.2%	31.5%
W9	62	1300	1257	-3.3%	64	1325	1264	-4.6%	39.8%
W8	64	1329	1308	-1.6%	65	1353	1305	-3.5%	28.5%
W7	70	1404	1361	-3.1%	70	1413	1355	-4.1%	46.2%
W6	72	1465	1437	-1.9%	72	1469	1418	-3.5%	50.2%
W4	74	1499	1497	-0.2%	74	1500	1463	-2.5%	29.0%
W5	78	1538	1462	-5.0%	77	1524	1497	-1.8%	46.8%
W3	79	1601	1552	-3.0%	79	1537	1544	0.5%	36.5%
W2	80/81	1627	1576	-3.1%	80	1588	1612	1.5%	28.2%
W1	83	1669	1616	-3.2%	82	1646	1636	-0.6%	41.7%

Table S1. NATAH•$^{+}$ mode assignments and frequencies derived from calculations ("calc.") or experiments ("obs.") on NATAH and NATAH•$^{+}$. Frequencies are given in cm^{-1}. Percentage difference between experimental and calculated frequencies is given as "% Error". Mode similarities were calculated using an internet-based application to analyze vibrational modes.[4] NA indicates a mode that was not assigned.

Mode	$\nu_{NATAH\bullet+}$ calc.	$\nu_{TrpH\bullet+}$ calc.	$\nu_{TrpH\bullet+}$ obs.	Δ D_2O calc.	Δ D_2O obs.	Δ d^5-Trp calc.	Δ d^5-Trp obs.	$\nu_{TrpH\bullet+}$ calc.[a]	$\nu_{TrpH\bullet+}$ obs.[b]	$\nu_{TrpH\bullet+}$ obs.[c]
W18	773	777	NA	-5	NA	-49	NA	746	753	NA
W17	881	893	884	-21	-2	-69	-54	851	NA	NA
W16	1039	1043	NA	0	NA	-189	NA	NA	1008	NA
W14	1178	1184	1140	-44	-5	-20	NA	1074	1170	NA
W13	1113	1118	NA	-4	NA	3	NA	NA	NA	NA
W12	1222	1224	NA	-13	NA	-50	NA	NA	NA	NA
W11	1246	1246	NA	15	NA	-10	NA	NA	NA	NA
W10	1216	1221	1164	5	-3	-326	-290	NA	NA	NA
W9	1325	1313	1264	-19	6	2	NA	NA	NA	NA
W8	1353	1362	1307	-16	10	-13	-21	1258 / 1350	NA	NA
W7	1413	1407	1361	-4	-6	-15	NA	1358	1283 / 1328	NA
W6	1469	1465	1418	-50	-52	-73	-78	1443	NA	NA
W5	1524	1531	1495	-19	-7	-47	-25	1459	1434	NA
W4	1500	1502	1467	-12	-10	-79	NA	1481	1522	NA
W3	1537	1549	1542	-3	-2	-10	-29	1459 / 1040	NA	NA
W2	1588	1606	1610	0	0	-25	-19	1550	1593	NA
W1	1646	1647	1635	-8	-4	-25	-20	1581	1646	1609

Table S2. Comparison of vibrational frequencies of NATAH$\bullet^+$ and TrpH$\bullet^+$ and predicted shifts for TrpH$\bullet^+$ with different isotopes. Calculated vibrational frequencies are indicated "calc." and experimental values are labeled "obs.". Isotope shift upon deuteration of the indole N-H is indicated as Δ D_2O, which is equal to ν(TrpD$\bullet^+$) (not shown) minus ν(TrpH$\bullet^+$). Calculated and observed isotope shifts upon perdeuteration of the indole ring are indicated as Δ d^5-Trp, and are equal to ν(d^5-TrpH$\bullet^+$) (not shown) minus ν(h^5-TrpH$\bullet^+$) (not shown). All values are reported in cm^{-1}; NA indicates not observed and/or assigned. [a,b,c]Results for TrpH$\bullet^+$ calculated and observed in references a[9], b[7], or c[8] are included.

Absorption spectrum and resonance Raman intensity maxima perturbed by intermolecular interactions

As discussed in the main text, the absorption spectrum and resonance Raman excitation profile of NATAH•$^+$ and TrpH•$^+$ appear to be blueshifted by ~3600 cm^{-1} (from 560 nm to 465 nm) from previously reported values of absorption spectra from TrpH•$^+$ in proteins and model compounds.[15-17] The effects of ion pairing on the absorption spectra of aromatic radicals have been studied previously, predominantly with time-resolved spectroscopy with photoionization or pulse radiolysis.[18-22] The radical anion of benzophenone in the presence of an amine cation exhibits an absorption maximum that is blue-shifted by up to 700 cm^{-1} in an organic solvent.[18] Addition of substoichiometric amount of sodium or lithium salts results in blue-shifts of 1000 cm^{-1} and 1750 cm^{-1}, respectively, while excess salt concentrations further shift the spectrum.[23] Photogenerated benzophenone radicals in hydrogen-bonding solvents exhibit more pronounced hypsochromic shifts, up to 2600 cm^{-1}, with increases in energy correlating to the increased hydrogen bonding strength of the solvent. Another example of the effects of ion pairing on absorption spectra is the fluorenone radical anion in the presence of sodium ions; the free radical ion absorbs at 570 nm while the presence of a contact ion pair increases the absorption energy by ~2100 cm^{-1}.[21] In the experiments presented here, the solvent is an excellent hydrogen bond partner and there are solvated sulfate ions in at least 400-fold excess relative to the NATA cation radical; therefore, ion pairing between the delocalized cation and the large sulfate anion may give rise to the observed blue-shift in the absorption spectrum. The dependence of the absorption spectrum on sulfate concentration lends support to this hypothesis. Hydrogen bonding of the radical cation to solvent may also have an effect.

Another intermolecular interaction to be considered is self-association of the NATAH radical cation. In polycyclic aromatic systems such as perylene and tetracene, it has been shown that dimerization of the radical cations can occur in sulfuric acid.[24] The dimer of perylene exhibits a blue-shift of the visible absorption band by 1300 cm^{-1} while the near-infrared absorption band of tetracene blueshifts by 1700 cm^{-1} upon dimerization. This dimerization has been shown to occur even when the radical cations are at concentrations of ~300 μM; the high dielectric constant of the solvent as well as delocalization of the charge over the aromatic pi system are thought to mitigate the electrostatic repulsion of the two cationic species.[24] However, this reference also rejects the possibility of ion pairing between the cation radicals and the sulfate anions in solution,[24] which contrasts with the above-mentioned results on ionic radical interactions with alkali cations.[23] It is evident that both of these contrasting mechanisms can impact the absorption spectrum of a radical ion, and it is not clear which effect will dominate in the $NATAH^{\bullet+}$/Ce(IV) system. Overall, because of the high ionic strength of the sulfuric acid solution, the possible effects of ion pairing between the aromatic cation and the inorganic anion cannot be ignored.

The polarity of the environment around NATA may also influence the apparent absorption spectrum of the radical cation. The dielectric of the matrix around polyaromatic hydrocarbon radical cations has recently been shown to play a significant effect on their electronic transitions.[25] Dissolving aromatic hydrocarbons such as anthracene in oleum, or fuming sulfuric acid, produces the one-electron oxidized radical cation species. In nearly all cases, the identity of the solvent results in a change in the lowest electronic transition relative to the absorption spectrum maximum in an inert Ar matrix; naphthalene shows a -550 cm^{-1} change in energy, while the transition energies of the larger radicals of anthracene, tetracene, and

pentacene increase by 2600 cm^{-1}, 3800 cm^{-1}, and 2600 cm^{-1} respectively. The order of magnitude of these shifts is similar to that observed for NATAH$\bullet^{+}$ here.

There are a number of differences between the conditions under which NATAH$\bullet^{+}$ is generated in these experiments and previously observed TrpH$\bullet^{+}$ absorption spectra in proteins or model compounds.[15-17] The collective effects of high concentration, self-association, ion pairing, hydrogen bonding, and the high dielectric of the medium may act cumulatively to give rise to the observed hypsochromic shift of the absorption spectrum of NATAH$\bullet^{+}$. Future experiments and additional calculations are underway to identify the molecular mechanism that is responsible for this shift.

Supplemental discussion on vibrational mode enhancement pattern

The resonance enhancement mechanism relies on normal modes that are coupled to the electronically excited state; this coupling may help explain the significant difference in intensity patterns between the cation radical and closed-shell species. The closed-shell UVRR spectrum of NATA is obtained via excitation into a high-lying electronic state, the B_b band, to avoid interference from fluorescence emission at longer wavelengths. This spectrum shows largest peak intensities primarily in the low-frequency (<1000 cm^{-1}) region (Figure 1). In contrast, the resonance Raman spectrum of NATAH$\bullet^{+}$ is obtained with excitation into the lowest-lying electronic state and high-frequency peaks dominate the spectrum. This mode enhancement pattern likely reflects the differences in the excited states that are accessed; UVRR spectra of tryptophan excited into the lower energy electronic state show a similar enhancement pattern.[26]

Additional support that the observed species is the tryptophan-derived cation radical

We also investigated the possibility that the product probed in the RR experiments is not the isolated tryptophan cation radical. Multistep oxidation of organic substrates has been observed using cerium sulfate. This process proceeds through an initial radical cation step,[27] but the subsequent decomposition pathways require additional equivalents of cerium(IV).[28] In the system reported here, only a single equivalent of cerium(IV) is used, which limits further reaction of the tryptophan-derived cation radical. The back reaction of Ce(III) with $TrpH^{\bullet+}$ is thermodynamically unfavorable, and cerium will not participate in a chemical reaction to form a covalent bond within the indole manifold. The delay times used here range from 100 ms to 1 s, and are similar to those used in the fast-flow mixing electron paramagnetic resonance (EPR) experiment on which this current experiment is based.[29] Initially, the mixing product was studied via RR spectroscopy at approximately the same time delay as the EPR experiments to confirm that the observed bands reflect the tryptophan cation radical; the current experiments were then optimized to obtain maximum RR signal. One reason for the discrepancy in optimal probe times between EPR and RR experiments may reflect the different, and perhaps inferior, design of our mixing device relative to that used in EPR experiments.[29] Furthermore, while tryptophan has been shown to react with reactive oxygen species and dioxygenase enzymes to produce oxidized products such as N-formylkynurenine (NFK), kynurenine, and hydroxy-substituted species, these are slow, multistep processes that require oxygen.[30-36] In the present experiments, oxygen is excluded from the reaction mixture by extensive sparging with nitrogen, the reaction product is evident at times as short as ~100 ms after mixing, and the new peaks disappear altogether if the reagents are not continuously flowing or if a pre-mixed solution of NATA and cerium sulfate is introduced into the probe beam (Figure S8). The signal intensity is

independent of dissolved oxygen concentration (<1 μM – 1.5 mM dissolved O_2 in H_2SO_4),[37] and the absorption spectrum of the waste generated after mixing NATA with Ce(IV) predominantly reflects closed-shell NATA, with no absorption bands at 318 nm and 361 nm that would reflect the irreversible oxygen-addition products to tryptophan, NFK and kynurenine, respectively.[30] Finally, the vibrational frequencies of both NFK and kynurenine differ significantly from the vibrational frequencies of NATAH$\bullet^+$ that are reported here (Figure S11), and the product of kynurenine oxidation with Ce(IV) also displays distinct vibrational signatures from those reported here for NATAH$\bullet^+$ (Figure S12).[30] Overall, these control experiments support the claim that the vibrational modes observed in the resonance Raman experiments reflect those of the tryptophan-derived cation radical.

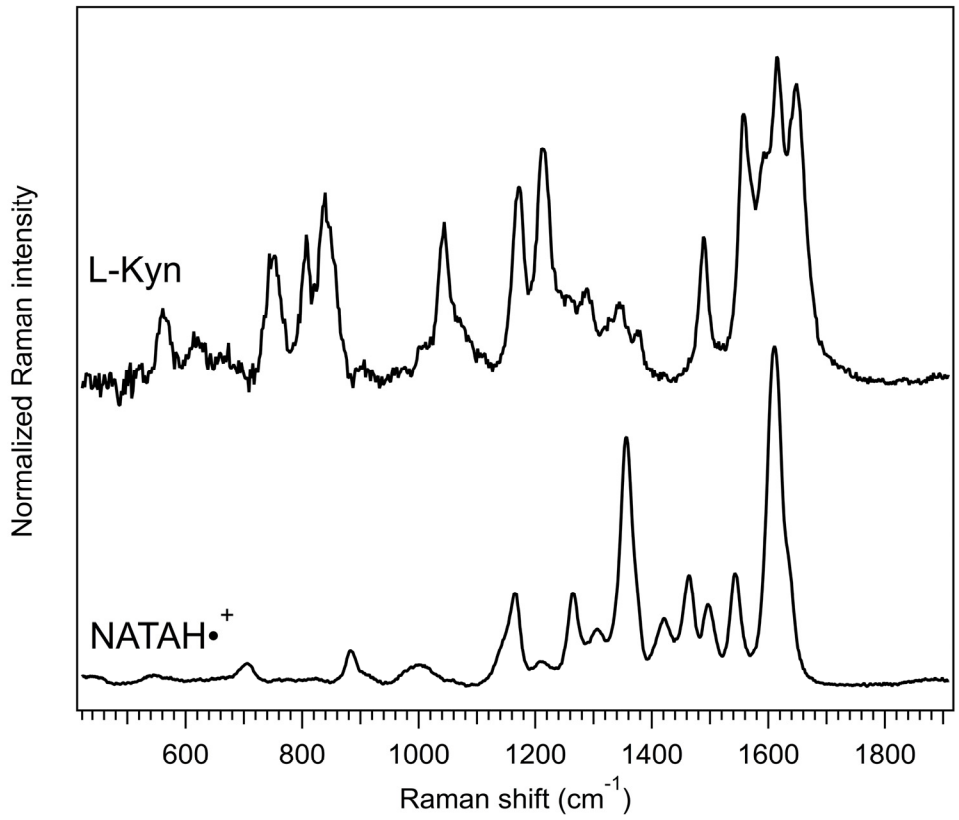

Figure S11. Resonance Raman spectra of kynurenine (L-Kyn) with 228 nm excitation in aqueous buffer (20 mM phosphate buffer, pH 7.2) and NATAH•$^{+}$ with 514.5 nm excitation in 225 mM H_2SO_4 in the presence of 500 μM $Ce^{IV}(SO_4)_2$.

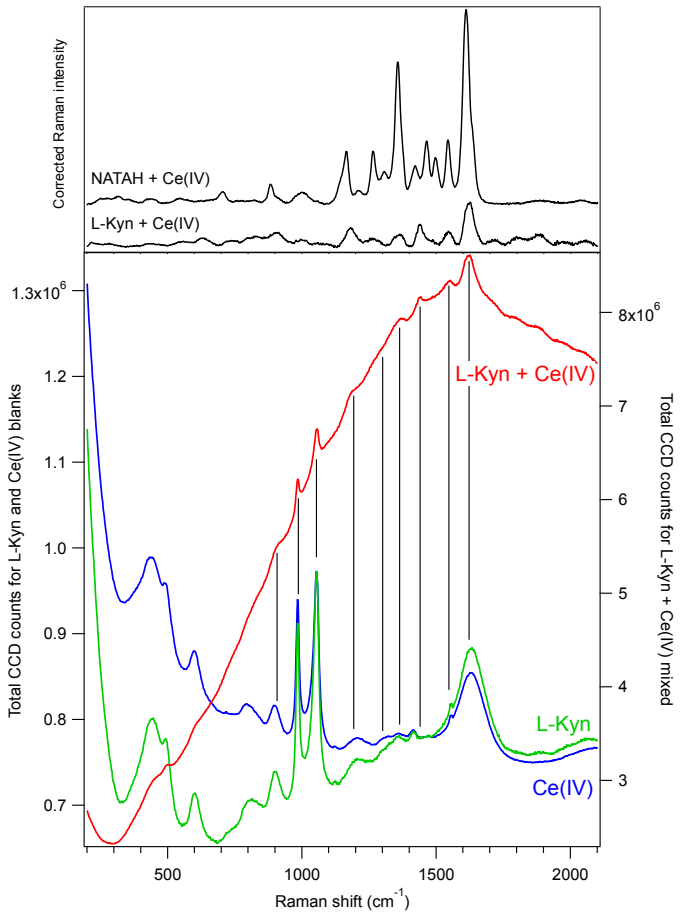

Figure S12. (Top) Raman spectra (514.5 nm excitation) of kynurenine (L-Kyn) and NATAH in 225 mM H_2SO_4 upon mixing with 500 µM $Ce^{IV}(SO_4)_2$. Spectra have been corrected by subtracting appropriate blank spectra until the sulfate peaks disappeared. Broad fluorescence backgrounds have also been removed. (Bottom) Raw Raman spectra of L-Kyn in 225 mM H_2SO_4 upon mixing with 500 µM $Ce^{IV}(SO_4)_2$ (right axis) along with corresponding spectra of L-Kyn and $Ce^{IV}(SO_4)_2$ blanks (left axis). All features in the residual spectrum of L-Kyn + $Ce^{IV}(SO_4)_2$ in the top panel are present in the control blanks.

References

1. Sanchez, K. M.; Neary, T. J.; Kim, J. E., Ultraviolet Resonance Raman Spectroscopy of Folded and Unfolded States of an Integral Membrane Protein. *J. Phys. Chem. B* **2008,** *112* (31), 9507-9511.
2. Shafaat, H. S. Spectroscopy and dynamics of amino acid radical intermediates in electron transfer processes. University of California, San Diego, La Jolla, 2011.
3. Frisch, M. J. T., G. W.; Schlegel, H. B.; Scuseria, G. E.; Robb, M. A.; Cheeseman, J. R.; Scalmani, G.; Barone, V.; Mennucci, B.; Petersson, G. A.; Nakatsuji, H.; Caricato, M.; Li, X.; Hratchian, H. P.; Izmaylov, A. F.; Bloino, J.; Zheng, G.; Sonnenberg, J. L.; Hada, M.; Ehara, M.; Toyota, K.; Fukuda, R.; Hasegawa, J.; Ishida, M.; Nakajima, T.; Honda, Y.; Kitao, O.; Nakai, H.; Vreven, T.; Montgomery, Jr., J. A.; Peralta, J. E.; Ogliaro, F.; Bearpark, M.; Heyd, J. J.; Brothers, E.; Kudin, K. N.; Staroverov, V. N.; Kobayashi, R.; Normand, J.; Raghavachari, K.; Rendell, A.; Burant, J. C.; Iyengar, S. S.; Tomasi, J.; Cossi, M.; Rega, N.; Millam, N. J.; Klene, M.; Knox, J. E.; Cross, J. B.; Bakken, V.; Adamo, C.; Jaramillo, J.; Gomperts, R.; Stratmann, R. E.; Yazyev, O.; Austin, A. J.; Cammi, R.; Pomelli, C.; Ochterski, J. W.; Martin, R. L.; Morokuma, K.; Zakrzewski, V. G.; Voth, G. A.; Salvador, P.; Dannenberg, J. J.; Dapprich, S.; Daniels, A. D.; Farkas, Ö.; Foresman, J. B.; Ortiz, J. V.; Cioslowski, J.; Fox, D. J. *Gaussian 09 Revision A.1*, Gaussian Inc.: Wallingford, CT, 2009.
4. Grafton, A. K., Vibalizer: A Free, Web-Based Tool For Rapid, Quantitative Comparison And Analysis Of Calculated Vibrational Modes. *J. Comput. Chem.* **2007,** *28* (7), 1290-1305.
5. Shafaat, H. S.; Leigh, B. S.; Tauber, M. J.; Kim, J. E., Resonance Raman Characterization of a Stable Tryptophan Radical in an Azurin Mutant. *J. Phys. Chem. B* **2009,** *113* (1), 382-388.
6. Harada, I.; Takeuchi, H., Raman and Ultraviolet Resonance Raman Spectra of Proteins and Related Compounds. In *Spectroscopy of Biological Systems*, Clark, R. J. H.; Hester, R. E., Eds. John Wiley and Sons Ltd: Chichester, U.K., 1986.
7. Johnson, C. R.; Ludwig, M.; Asher, S. A., Ultraviolet Resonance Raman Characterization Of Photochemical Transients Of Phenol, Tyrosine, And Tryptophan. *J. Am. Chem. Soc.* **1986,** *108* (5), 905-912.
8. Bisby, R. H.; Johnson, S. A.; Parker, A. W.; Tavender, S. M., Time-Resolved Resonance Raman Spectroscopy Of Indolyl And Related Radicals. *RAL Technical Reports* **1995,** *RAL-TR-95-025*.
9. Walden, S. E.; Wheeler, R. A., Structural And Vibrational Analysis Of Indolyl Radical And Indolyl Radical Cation From Density Functional Methods. *J. Chem. Soc., Perkin Trans. 2* **1996,** (12), 2663-2672.
10. Dieng, S. D.; Schelvis, J. P. M., Analysis of Measured and Calculated Raman Spectra of Indole, 3-Methylindole, and Tryptophan on the Basis of Observed and Predicted Isotope Shifts. *J. Phys. Chem. A* **2010,** *114* (40), 10897.
11. Crespo, A.; Turjanski, A. G.; Estrin, D. A., Electronic Spectra Of Indolyl Radicals: A Time-Dependent DFT Study. *Chem. Phys. Lett.* **2002,** *365* (1-2), 15-21.
12. Walden, S. E.; Wheeler, R. A., First Evidence Of Anchimeric Spin Delocalization In Tryptophan Radical Cation. *J. Am. Chem. Soc.* **1997,** *119* (13), 3175-3176.
13. Ayala, I.; Range, K.; York, D.; Barry, B. A., Spectroscopic Properties Of Tyrosyl Radicals In Dipeptides. *J. Am. Chem. Soc.* **2002,** *124* (19), 5496-5505.
14. Pujols-Ayala, I.; Sacksteder, C. A.; Barry, B. A., Redox-Active Tyrosine Residues: Role For The Peptide Bond In Electron Transfer. *J. Am. Chem. Soc.* **2003,** *125* (25), 7536-7538.

15. Solar, S.; Getoff, N.; Surdhar, P. S.; Armstrong, D. A.; Singh, A., Oxidation Of Tryptophan And N-Methylindole By $N_3^{\bullet -}$, $Br_2^{\bullet -}$, And $(SCN)_2^{\bullet -}$ Radicals In Light- And Heavy-Water Solutions: A Pulse Radiolysis Study. *J. Phys. Chem.* **1991,** *95* (9), 3639-3643.
16. Stevenson, K. L.; Papadantonakis, G. A.; LeBreton, P. R., Nanosecond UV Laser Photoionization Of Aqueous Tryptophan: Temperature Dependence Of Quantum Yield, Mechanism, And Kinetics Of Hydrated Electron Decay. *J. Photochem. Photobiol., A* **2000,** *133* (3), 159-167.
17. Byrdin, M.; Villette, S.; Espagne, A.; Eker, A. P. M.; Brettel, K., Polarized Transient Absorption To Resolve Electron Transfer Between Tryptophans In DNA Photolyase. *J. Phys. Chem. B* **2008,** *112* (22), 6866-6871.
18. Simon, J. D.; Peters, K. S., Solvent Effects On The Picosecond Dynamics Of The Photo-Reduction Of Benzophenone By Aromatic-Amines. *J. Am. Chem. Soc.* **1981,** *103* (21), 6403-6406.
19. Simon, J. D.; Peters, K. S., Direct Observation Of The Special Salt Effect - Picosecond Dynamics Of Ion-Pair Exchange. *J. Am. Chem. Soc.* **1982,** *104* (22), 6142-6144.
20. Simon, J. D.; Peters, K. S., Picosecond Dynamics Of Ion-Pairs - The Effect Of Hydrogen-Bonding On Ion-Pair Intermediates. *J. Am. Chem. Soc.* **1982,** *104* (24), 6542-6547.
21. Gersdorf, J.; Mattay, J., Photoreactions Of Fluorenone With Electron-Rich Alkenes: Radical Ion Pair Formation In Polar And Non-Polar Solvents. *Journal of Photochemistry* **1985,** *28* (3), 405-411.
22. Yamamoto, Y.; Aoyama, T.; Hayashi, K., Pulse-Radiolysis Study Of Salt Effects On Reactions Of Aromatic Radical Cations With Cl- .2. Spectral Shifts And Decay Kinetics Of Diphenylpolyene Radical Cations In The Presence Of Tetrabutylammonium Hexafluorophosphate. *Journal Of The Chemical Society-Faraday Transactions I* **1988,** *84*, 2209-2214.
23. Simon, J. D.; Peters, K. S., Na+ And Li+ Effects On The Photo-Reduction Of Benzophenone - A Picosecond Absorption Study. *J. Am. Chem. Soc.* **1983,** *105* (15), 4875-4882.
24. Kimura, K.; Yamazaki, T.; Katsumat.S, Dimerization Of Perylene And Tetracene Radical Cations And Electronic Absorption Spectra Of Their Dimers. *J. Phys. Chem.* **1971,** *75* (12), 1768-1774.
25. Cataldo, F.; Iglesias-Groth, S.; Manchado, A., Electronic Absorption Spectroscopy Of Polycyclic Aromatic Hydrocarbons (Pahs) Radical Cations Generated In Oleum: A Superacid Medium. *Spectrochim. Acta, Part A 77* (5), 998-1004.
26. Austin, J. C.; Rodgers, K. R.; Spiro, T. G., Protein-Structure From Ultraviolet Resonance Raman-Spectroscopy. *Metallobiochemistry, Part C* **1993,** *226*, 374-396.
27. Paulenova, A.; Creager, S. E.; Navratil, J. D.; Wei, Y., Redox Potentials And Kinetics Of The Ce3+/Ce4+ Redox Reaction And Solubility Of Cerium Sulfates In Sulfuric Acid Solutions. *J. Power Sources* **2002,** *109* (2), 431-438.
28. Bhatt, M. V.; Periasamy, M., Kinetics Of Ceric Ion Oxidation Of Naphthalene And Its Derivatives - Formation Of The Radical-Cation Intermediate In The Rate-Limiting Step. *J. Chem. Soc., Perkin Trans. 2* **1993,** (10), 1811-1814.
29. Connor, H. D.; Sturgeon, B. E.; Mottley, C.; Sipe, H. J.; Mason, R. P., L-Tryptophan Radical Cation Electron Spin Resonance Studies: Connecting Solution-Derived Hyperfine Coupling Constants With Protein Spectral Interpretations. *J. Am. Chem. Soc.* **2008,** *130* (20), 6381-6387.

30. Dreaden, T. M.; Chen, J.; Rexroth, S.; Barry, B. A., N-Formyl Kynurenine As A Marker Of High Light Stress In Photosynthesis. *J. Biol. Chem.* **2011**.
31. Ehrenshaft, M.; de Oliveira Silva, S.; Perdivara, I.; Bilski, P.; Sik, R. H.; Chignell, C. F.; Tomer, K. B.; Mason, R. P., Immunological Detection Of N-Formylkynurenine In Oxidized Proteins. *Free Rad. Biol. & Med.* **2009,** *46* (9), 1260.
32. Schmidt, H.; Bieker, L., Raman-Spectra Of Chemically Modified Lysozyme - Oxindole Derivatives. *Arch. Biochem. Biophys.* **1979,** *195* (1), 205-210.
33. Gracanin, M.; Hawkins, C. L.; Pattison, D. I.; Davies, M. J., Singlet-Oxygen-Mediated Amino Acid And Protein Oxidation: Formation Of Tryptophan Peroxides And Decomposition Products. *Free Rad. Biol. & Med.* **2009,** *47* (1), 92-102.
34. Efimov, I.; Basran, J.; Thackray, S. J.; Handa, S.; Mowat, C. G.; Raven, E. L., Structure and Reaction Mechanism in the Heme Dioxygenases. *Biochemistry 50* (14), 2717-2724.
35. Rafice, S. A.; Chauhan, N.; Efimov, I.; Basran, J.; Raven, E. L., Oxidation Of L-Tryptophan In Biology: A Comparison Between Tryptophan 2,3-Dioxygenase And Indoleamine 2,3-Dioxygenase. *Biochem. Soc. Trans.* **2009,** *37*, 408-412.
36. Basran, J.; Rafice, S. A.; Chauhan, N.; Efimov, I.; Cheesman, M. R.; Ghamsari, L.; Raven, E. L., A Kinetic, Spectroscopic, and Redox Study of Human Tryptophan 2,3-Dioxygenase *Biochemistry* **2008,** *47* (16), 4752-4760.
37. Hitchman, M. L., *Measurement of Dissolved Oxygen*. Krieger Publishing Company: 1988.